Temporal and Spatial Combining for 5G mmWave Small Cells

This chapter proposes the combination of temporal processing through Rake combining based on direct sequence-spread spectrum (DS-SS), and multiple antenna beamforming or antenna spatial diversity as a possible physical layer access technique for fifth generation (5G) small cell base stations (SBS) operating in the millimetre wave (mmWave) frequencies. Unlike earlier works in the literature aimed at previous generation wireless, the use of the beamforming is presented as operating in the radio frequency (RF) domain, rather than the baseband domain, to minimise power expenditure as a more suitable method for 5G small cells. Some potential limitations associated with massive multiple input-multiple output (MIMO) for small cells are discussed relating to the likely limitation on available antennas and resultant beamwidth. Rather than relying, solely, on expensive and potentially power hungry massive MIMO (which in the case of a SBS for indoor use will be limited by a physically small form factor) the use of a limited number of antennas, complimented with Rake combining, or antenna diversity is given consideration for short distance indoor communications for both the SBS) and user equipment (UE). The proposal's aim is twofold: to solve eroded path loss due to the effective antenna aperture reduction and to satisfy sensitivity to blockages and multipath dispersion in indoor, small coverage area base stations. Two candidate architectures are proposed. With higher data rates, more rigorous analysis of circuit power and its effect on energy efficiency (EE) is provided. A detailed investigation is provided into the likely design and signal processing requirements. Finally, the proposed architectures are compared to current fourth generation long term evolution (LTE) MIMO technologies for their anticipated power consumption and EE.

David Muirhead
Honeywell Aerospace
Tewkesbury UK

Muhammad Ali Imran
School of Engineering
University of Glasgow, UK

1.1 Introduction

In line with current thinking that 5G is unlikely to be satisfied with a 'one fits all' single air interface or access technology approach [1], specific investigation of the physical layer targeted for indoor and densely deployed SBSs warrants analysis. 5G opens the door to a range of connected technologies that are not confined to conventional mobile broadband (MBB) but may be applicable to SBSs. Application areas falling under the new category of machine type communications (MTC) will set further requirements on the air interface technology. Mission critical latencies, low energy, high reliability, high availability are new challenges in addition to high spectral efficiency and increased data rates for MBB [2]. High availability will require significant resilience to failure and with non-line of sight (NLOS) propagation being possible mmWave, combating the effects of multipath dispersion caused by reflection is important. Examples of recent air interface research for 5G consider the use of orthogonal frequency division multiplexing (OFDM) based techniques [3][4], the work presented here is in contrast to this and considers alternative approach based on DS-SS, specifically for the SBS.

1.1.1 Conventional Massive MIMO 5G Architectures

Massive MIMO or large scale antenna systems (LSAS) has been a research focus since the pivotal paper from Marzettta [5]. The premise is that the number of base station antennas N is much larger than the number of single antenna terminals, K [6]. In addition to combating eroded link margin due to reduced antenna aperture, the many antennas helps the multipath problem. When the data rate increases the symbol duration decreases. If the multipath delay spread is greater than the symbol length, complex equalization is required to combat the effects of inter-symbol interference (ISI). To overcome this, beam steering/forming is suggested to minimise the spatial footprint of the channel resulting in a more favourable multipath profile thus constraining the ISI problem. Antenna directivity is thus used to minimise the effects of ISI.

Many researchers are optimistic that the gains provided by massive MIMO will facilitate simple receiver architectures through low complexity waveforms [7] e.g. quadrature phase shift keying (QPSK). Such receivers would comprise simple matched filters, not requiring expensive and complex signal processing in the form of equalization. However, there are drawbacks. As an example, the amount of channel estimation required to formulate appropriate beamforming weights, required for either RF or digital beamforming, will be significant and will impact complexity and power. For frequency division duplex systems (FDD) this will be particularly acute. Furthermore, NLOS communication and channel blocking effects are a cause for concern. Reliability of a system purely based on beamforming might be challenging since the coverage might be more sensitive to both time and space variations [1]. Considering the spatial footprint or capture of an antenna system we refer to its beamwidth. As is discussed in [8] for an antenna configuration with a half power beamwidth (HPBW) of 6.5°, reliable communication is difficult to establish even for LOS at 60GHz and the movement of people can easily block and attenuate such a narrowbeam signal.

It is widely accepted that the use of mmWave for short indoor distances, is subject to multipath dispersion due to blockages [7][9]. In this case NLOS communication may be the only possible means to overcome such effects. Beamforming may be inadequate in this situation if the blockage causes a significantly large attenuation and dispersion of the transmitted signal that the multipath components appear outside of the main antenna beam. Here, re-acquisition, identification and further antenna steering or beamforming may be required to find any available multipath energy.

Considering a uniform linear array (ULA) antenna array, an antenna array with uniform antenna spacing, the HPBW can be determined from:

$$HBPW = 2\left[\frac{\pi}{2} - cos^{-1}\left(\frac{1.39\lambda}{\pi N\Delta}\right)\right] \tag{1.1}$$

where Δ is the element spacing in wavelengths (λ).

A highly directive beam pattern is illustrated in Figure 1.1 where the polar and directivity plots of a 256 element ULA operating at 72GHz, element spacing of 0.4 cm are provided. As can be seen a main lobe width at the HPBW point (-3dB) from the maximum of around 1-2˚ is given. Considering an office or apartment indoor area of 10m x10m where the maximum distance between the transmitter and receiver is 14m ($(10^2.10^2)^{1/2}$) a maximum round trip propagation delay of 93ns (2 . (dist/C)) would exist. Delay spread beyond this would be expected to be between 1 and 35ns based on the findings in [10]-[12] as shown in Table 1.1. This would imply that multipath information may exist off the main direct path and outside the main beamwidth lobe for the 256 element ULA.

Table 1.1 Indoor mmWave Delays Spread

Freq	TX-RX Distance (m) /Area type	Delay Spread (ns)	Antenna Type
60GHz	9.2/Modern office	20 [11]	Horn antenna
60GHz	13.51x7.81/office	18.08 [12]	Omni-directional
60GHz	13.51 x 7.81	1.05 [12]	Narrow beam
73GHz	6-46	35 [10]	Co-polarized (15˚ HPBW)
73GHz	6-46	20 [10]	Cross-polarized (15˚ HPBW)

1.1.2 Small Cell Problem

To minimize the effects outlined, it is desirable to make use of all available multipath energy, including instantaneous multipath from blocking, and use it in a constructive way. For the case of SBS, it is desirable to use a low number of antennas to minimise power expenditure. This is indeed a constraint placed on the design not only from a power perspective but because the physical form factor limits the design to use less antenna elements. Figure 1.2 - Figure 1.3 illustrate the radiation patterns more suitable for a SBS with fewer antenna elements. The plots assume the free space propagation without scatters, noise or fading. Figure 1.2 shows a 4 antenna ULA system operating at 28GHz with a 1cm element spacing. Figure 1.3 shows a 12 antenna ULA system operating at 72GHz with a 0.4cm spacing.

Much wider beamwidths are evident and the spatial profile of the antenna pattern will facilitate the capture of more multipath components as well as providing moderate amounts of beamforming gain suitable for small distances. The illustrations show HPBWs of 15˚ and 6˚ for 72 and 28GHz operation respectively. With the additional gain provided by the beamformer, the ISI problem still exists since the main lobe is sufficiently wide enough to reasonably expect multipath capture.

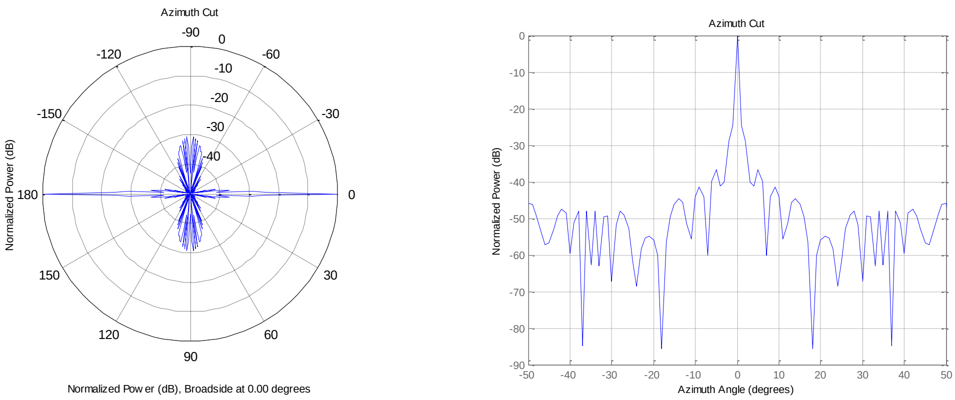

(a) (b)

Figure 1.1 256 Element, 72GHz - (a) Polar Plot, (b) Directivity Plot

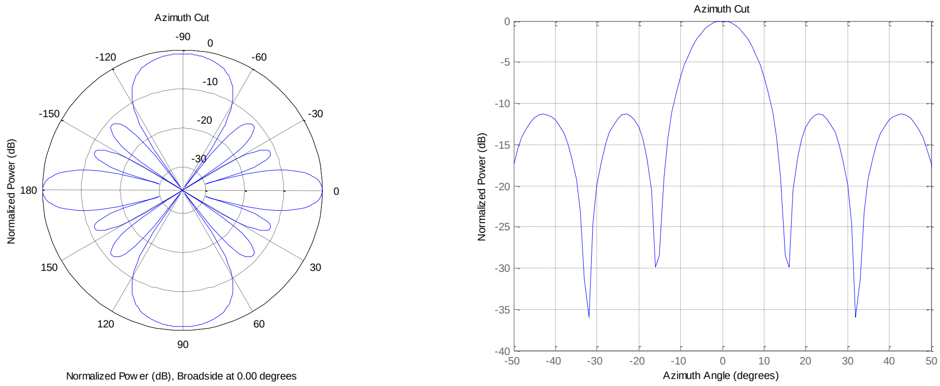

(a) (b)

Figure 1.2 Polar Plot, 4 Element, 28GHz - (a) Polar Plot, (b) Directivity Plot

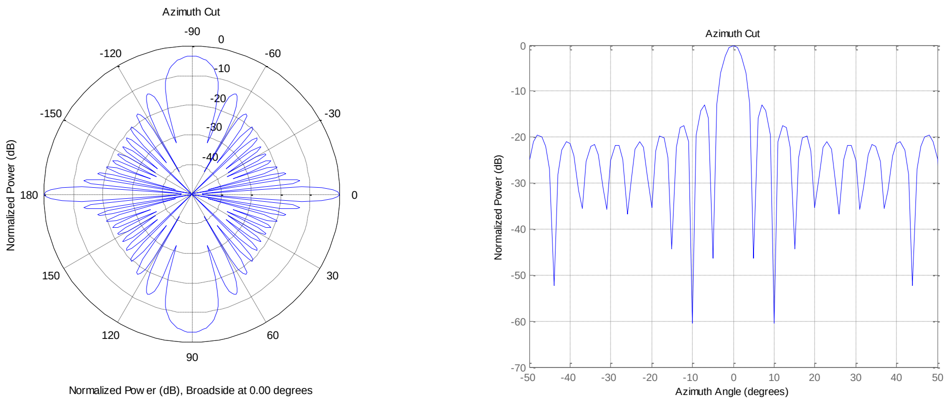

(a) (b)

Figure 1.3 Polar Plot, 12 Element, 72GHz - (a) Polar Plot, (b) Directivity Plot

1.2 Small Cell Physical Layer – 2D Rake Combiner

With the requirement to overcome eroded link margin but cater for likely multipath/NLOS communications in a low complexity and energy efficient manner an alternative architecture for the small cell is considered.

The use of Rake combining related techniques such as DS-SS for mmWave has been the subject of research in the literature. This has mainly been related to indoor and predominantly for 60GHz ultra wideband (UWB) home entertainment and multimedia systems [13] Joint use of multiple antenna beamforming for improved link margin together with Rake combining to combat the effects of ISI, thus providing performance gains in two dimensions, are proposed and analysed. A simplified architecture is proposed to satisfy the needs of the small cell. Research as recent as June 2015 advocates the use of

Rake combining techniques for indoor 60GHz operation [14]. However, such systems, despite claiming simple and low complex solutions, do not fully quantify the extent of this in terms of circuit power and EE. As part of the discussion presented here, a more quantifiable complexity and EE performance is given.

1.2.1 Direct Sequence-Spread Spectrum Rake Combining and mmWave

It is well known that in direct sequence-spread spectrum (DS-SS), information is transmitted using a wider bandwidth than necessary. Here data bits from the source $b(t)$ are multiplied by a code signal $c(t)$ at a faster rate known as the chip rate. The process is referred to as spreading and the amount of spreading is determined by the spreading factor (SF). At the receiver of such a system, the use of a Rake Receiver effectively performs the equalization task by combining the received signal with multiple, time delayed versions of it (the multipaths) separated by multiples of the chip period (T_c). This allows the components of the original signal to be recovered with the time delays removed. Maximum ratio combining (MRC) of the delayed signals yields an optimal output which has a maximum possible signal to noise ratio given the input signals [15]. Optimal performance is expected because the increased bandwidth of the spread signal allows the receiver to resolve multipath energy which would otherwise appear combined with a single channel tap in other systems. In this sense the spreading mechanism gives us the ability to find available energy and use it to our advantage. In particular, considering the spread signals with chip time T_c inversely proportional to the spreading bandwidth; in this case, the individual paths can be distinguished if they are mutually separated by delays greater than T_c. The various delayed versions of the signal will be mutually nearly uncorrelated [14]. Since the mmWave frequency bands permit the use of high bandwidth spreading, the corresponding multipath resolution will be significant (sub-nanosecond). This therefore increases the effective diversity order and much, if not all, available energy can be identified and used to increase the signal to noise ratio (SNR) of the signal.

To summarize, in most receiver design multipath creates inter symbol interference that requires potentially complex equalization techniques. In the case of DS-SS such multipath components can be used in a constructive way to improve the performance of the system by detecting and combining the main and delayed multipath components in a Rake Receiver. In this case multipath actually provides additional improvements in the system performance and resilience to NLOS communications. This therefore satisfies the requirement of using all available energy and addressing ISI in the likely transmission conditions of a 5G SBSs.

1.2.2 Spatial and Temporal Processing

Antenna arrays at the SBS can be utilized to form spatial domain beam patterns for both the UL and DL. This maximises the desired users signal. DS-SS provides temporal diversity gain through multipath combining. Thus, there are 2 dimensions, spatial and temporal, to increase the performance of the communications link in the proposed scheme. In operation the received signal is first cross-correlated with a local copy of the spreading sequence (combined with a scrambling code) such that the chip positions corresponding to the time delays of the required user can be identified [16]. A Rake combiner is used to equalise the main and time delayed multipath components to maximise the signal to interference ratio (SIR) of the signal. The use of beamforming in baseband will result in excessive power consumption because of the use of analogue to digital converters (ADC) behind each antenna element. In the following discussion, the use of beamforming is performed in RF domain followed by correlation in baseband is therefore proposed.

1.3 Transceiver Architectures

Since each user, in a DS-SS system is transmitted and received simultaneously at the SBS, (and identified by their unique scrambling code), the use of RF beamforming is potentially limited to providing the same antenna pattern for each user. In this case the beamforming gain can be used to sectorize a coverage area – see Figure 1.4. For the UE, RF beamforming offers a mechanism to improve the link margin by increasing the effective antenna aperture of the receiver, as well as the facilitation of transmit beamforming gain.

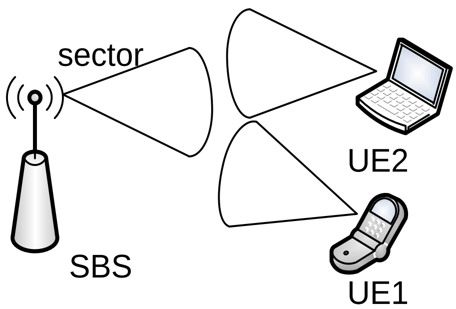

Figure 1.4 DL sectored and UL beamforming at SBS and UE

An alternative architecture, providing 360° coverage at the SBS, is to employ transmit and receive diversity techniques, rather than beamforming, illustrated in Figure 1.5, and provide user gain in the form of diversity gain in the DL and UL. Both BS and UE receive will employ digital antenna diversity with Rake combining.

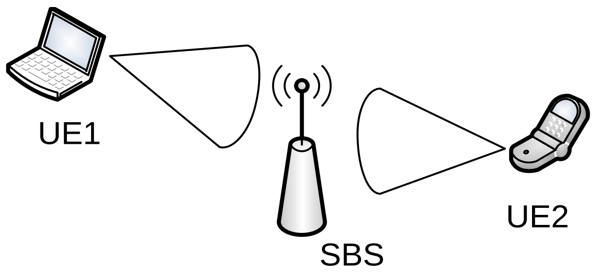

Figure 1.5 DL and UL antenna diversity at SBS for 360° coverage

Two transceiver architectures are considered and shown in Figure 1.6 and Figure 1.7 - Architecture 1 & 2. Both use DS-SS, but the utilisation of the antenna system is different. Architecture 1 considers

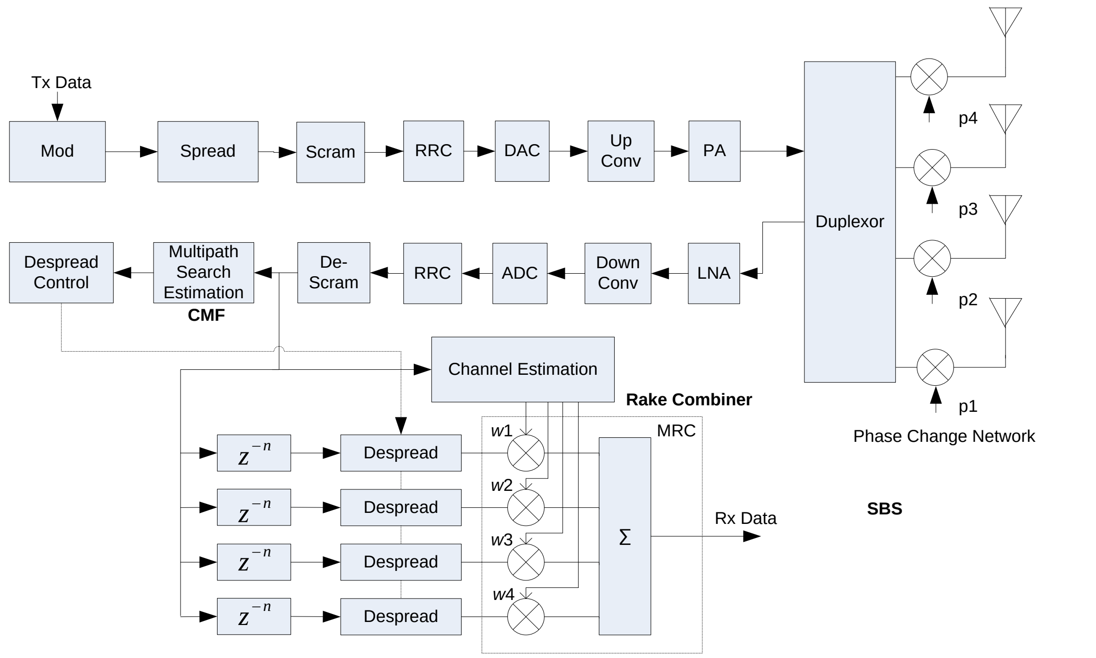

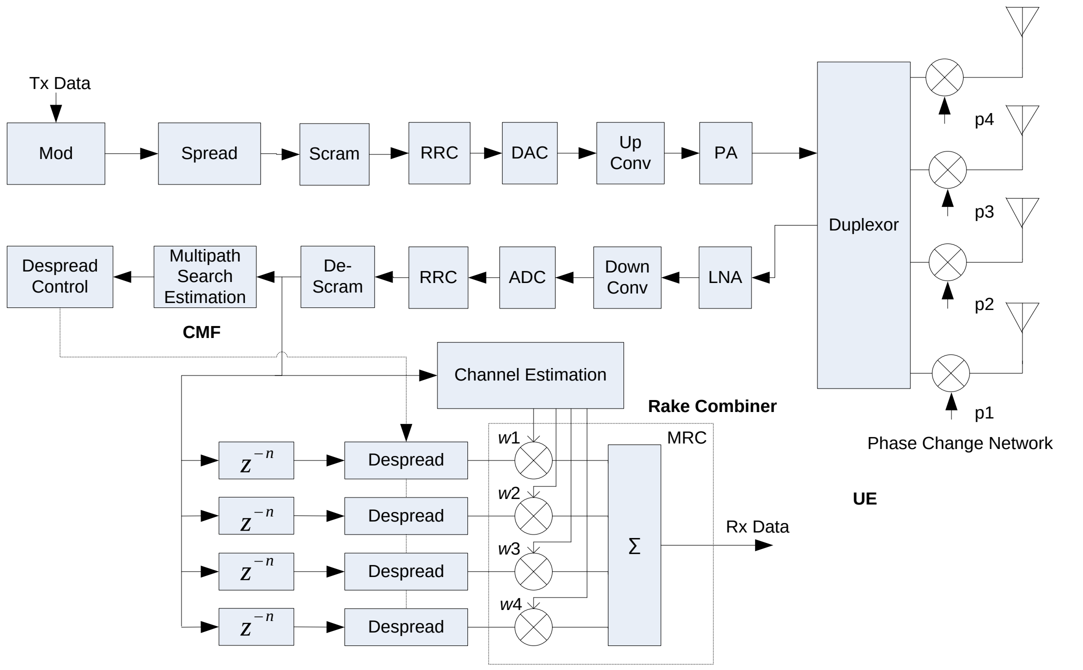

Figure 1.6 Architecture - 1

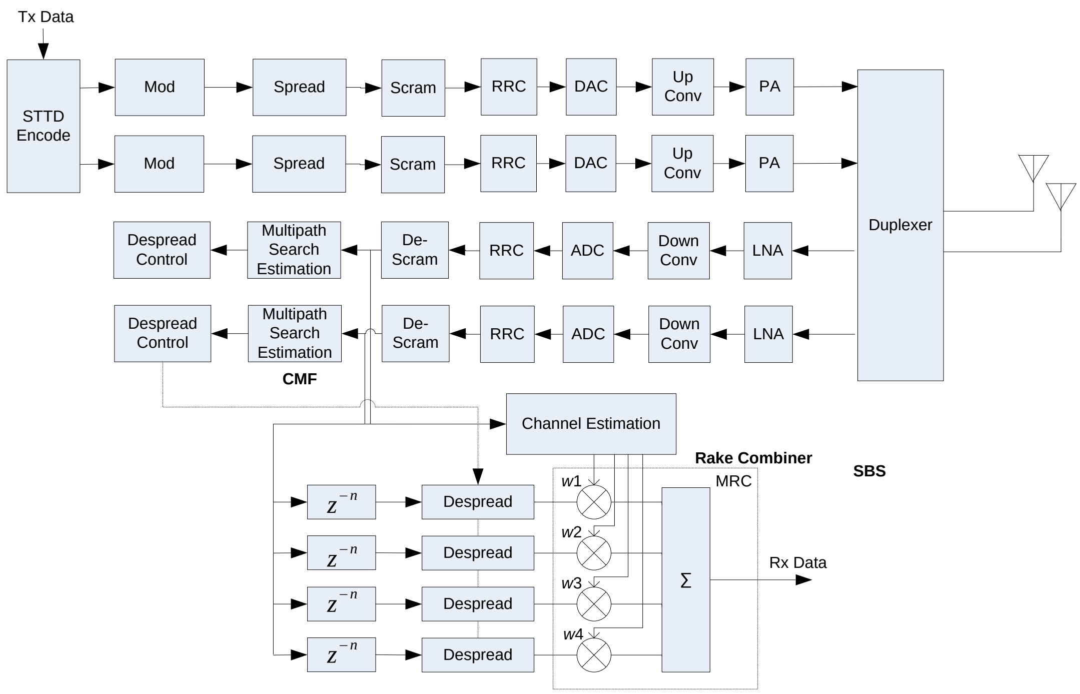

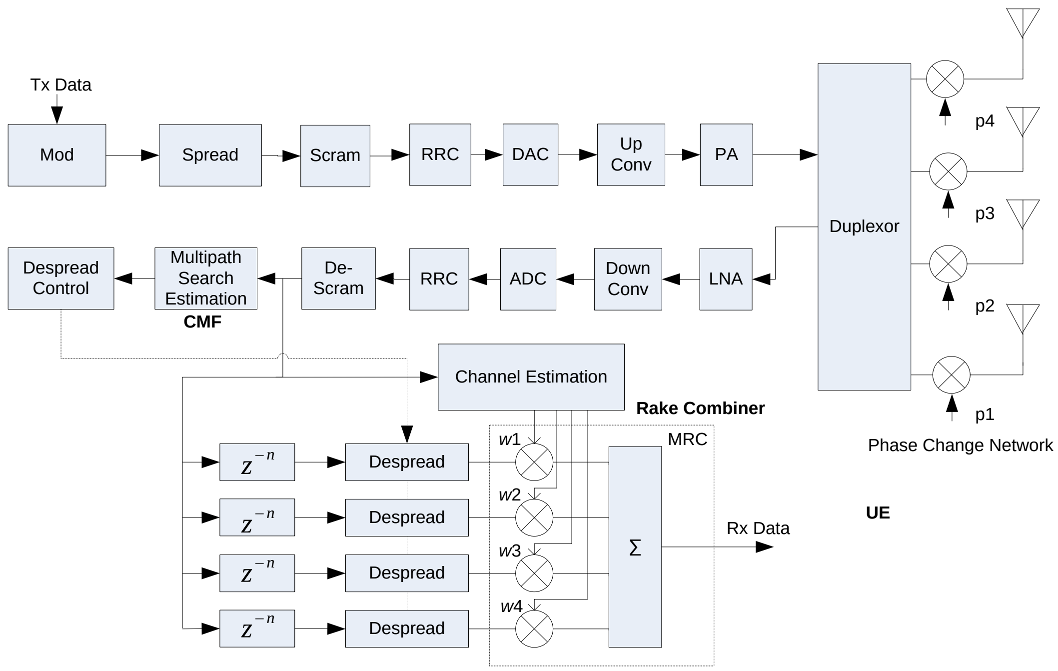

Figure 1.7 Architecture - 2

the use of an RF beamforming antenna array at the SBS and an antenna array providing beamforming in the RF domain at the UE. Architecture 2, shown in Figure 1.7, improves the transmit performance and receive gain of the BS by employing transmit and receive diversity at the expense of additional ADC/DACs. Both architectures comprise identical spreading, scrambling, filtering, and necessary up conversion and amplification in the transmit path. For Architecture 1, receive beamforming is provided across an N element array (N=2:4). Following the beamformer, amplification, down-conversion and corresponding descrambling and despreading is provided. Multipath search estimation is used to determine appropriate multipaths in the channel that are then combined in a Rake combiner. The identification and acquisition of multipath components is required to exploit their energy and it is particularly important to determine the relative delays and when possible their amplitude and phase components.

Identification of multipath elements in a transmission can be performed using the time domain correlator, implemented as a code matched filter (CMF), who's taps are equivalent to a local and known spreading and scrambling code sequence multiplied by known pilot symbols (for channel estimation). Assuming a single beamformed lobe, multipath search estimation complexity is determined by the number of expected multipaths or more precisely the timing uncertainty over which to search. In a small cell this should be low since it is constrained by the physical coverage area. A Rake combiner is used to combine the multipath components identified by the correlator. To summarise, the motivation and advantages of such a system are as follows:

I. Spreading allows the identification of time delayed multipath components by correlating the transmitted signal with a local copy of the spreading code (which will likely be combined a scrambling sequence and known pilots). In particular and with high bandwidth associated with mmWave spectrum, multipath resolution to sub-nanosecond accuracy is possible.
II. Unlike other systems, the multipaths in DS-SS can be used to perform constructive combining at the receiver with a Rake combiner. This therefore provides additional gain in the form of diversity gain and provides resistance to blocking and multipath dispersion.
III. Assuming that the number of users is limited in the small cell, the DS-SS system, which is normally limited by the maximum number of users will be less affected by multiple access interference (MAI) and noise rise.
IV. Large bandwidth exists in the mmWave bands to facilitate the additional spectrum needed by the spreading process.
V. The spreading and scrambling processes can be considered as low complexity. Arguably the most complex part is the time domain correlator but since its complexity is driven by delay spread this will be minimal in an indoor deployment where the distance will be small.
VI. DS-SS with low order modulations such as QPSK will facilitate low peak to average power ratio (PAPR) compared to more complex modulation envelopes or multi-carrier systems (such as OFDM. This will result in more efficient use of power amplifiers.
VII. A small cell radius could enable the use of lower power ADC/DAC through lower dynamic range requirements.

The disadvantage with such a scheme is the effective waste of bandwidth due to the spreading process i.e. for every symbol transmitted SF x system bandwidth is needed. Additionally, due to the higher effective signal bandwidth the ADC and DAC components will be required to clock yet higher meaning greater power consumption. In general it is preferred that the ADC has large spurious free dynamic range (SFDR) meaning large order ADC devices e.g. 12-bit [17]. However, to reduce power consumption the use of smaller dynamic range ADCs could be suitable for short distances. Unlike OFDM systems, DS-SS is a single carrier system meaning it has a lower peak-to-average power ratio (PAPR). Using low order modulation schemes such as binary phase shift keying (BPSK) or QPSK would allow the use of ADCs with a smaller dynamic range.

1.3.1 Performance Aspects

The link budget of a small cell based on the proposed 2D-Rake physical layer architecture 1 is shown in Table 1.2 and Table 1.3. Spreading factors of SF=4 and SF=8 are used. Particularly for the SF=4, the achievable data rates are comparable with those discussed in [18] which considers a single omni-directional antenna but due to the spreading and multipath combining, should provide better mitigation to blocking and the effects of channel. Table 1.2 and Table 1.3 show the achievable data rates when considering short distances between the transmitter and receiver. The data rate achievable are significant with only a four antennas at the receiver and a single transmit antenna element.

Table 1.2 2D-Rake Link Budget - SF4, 5 and 10m distance, 28 and 72GHz

Small Cell Link Budget	**Case1 sf4**	**Case2 sf4**	**Case3 sf4**	**Case3 sf42**
Tx Power (dBm)	20	20	20	20
Beamforming Gain (dBi)	12	12	12	12
Carrier Frequency (GHz)	2.80E+10	2.80E+10	7.20E+10	7.20E+10
Distance (m)	10	5	10	5
Propagation Loss (dB)	81.39688885	75.37628893	89.60037815	83.57977824
Spreading Factor	4	4	4	4
Other Losses	6	6	6	6
Received Power (dBm)	-55.39688885	-49.37628893	-63.60037815	-57.57977824
Bandwidth (GHz)	2.00E+09	2.00E+09	2.00E+09	2.00E+09
Thermal PSD (dBm/Hz)	-174	-174	-174	-174
Noise figure	10	10	10	10
Thermal Noise (dBm)	-7.10E+01	-7.10E+01	-7.10E+01	-7.10E+01
SNR (dB)	2.16E+01	2.76E+01	1.34E+01	1.94E+01
Implementation Loss (dB)	3	3	3	3
Data rate (bits/s)	3.10E+09	4.09E+09	1.79E+09	2.75E+09

Table 1.3 2D-Rake Link Budget – SF8, 5 and 10m distance, 28 and 72GHz

Small Cell Link Budget	**Case1 sf8**	**Case2 sf8**	**Case3 sf8**	**Case4 sf8**
Tx Power (dBm)	20	20	20	20
Beamforming Gain (dBi)	12	12	12	12
Carrier Frequency (GHz)	2.80E+10	2.80E+10	7.20E+10	7.20E+10
Distance (m)	10	5	10	5
Propagation Loss (dB)	81.39688885	75.37628893	89.60037815	83.57977824
Spreading Factor	8	8	8	8

Other Losses	6	6	6	6
Received Power (dBm)	- 55.39688885	-49.37628893	-63.60037815	-57.57977824
Bandwidth (GHz)	2.00E+09	2.00E+09	2.00E+09	2.00E+09
Thermal PSD (dBm/Hz)	-174	-174	-174	-174
Noise figure	10	10	10	10
Thermal Noise (dBm)	-7.10E+01	-7.10E+01	-7.10E+01	-7.10E+01
SNR (dB)	2.46E+01	3.06E+01	1.64E+01	2.24E+01
Implementation Loss (dB)	3	3	3	3
Data rate (bits/s)	1.80E+09	2.30E+09	1.13E+09	1.62E+09

1.3.2 Design and Complexity Aspects

As simple physical layer is suggested using QPSK modulated DS-SS. Using the 5G use case of sub-millisecond latency [19], a 500μs slot timing is used as shown in Figure 1.8. Each slot comprises data and pilot bits mapped to the real (I) and imaginary (Q) components of the signal respectively. Pilot symbols are used for parameter estimation of multipath components and channel state information (CSI) for appropriate weighting and receive functions.

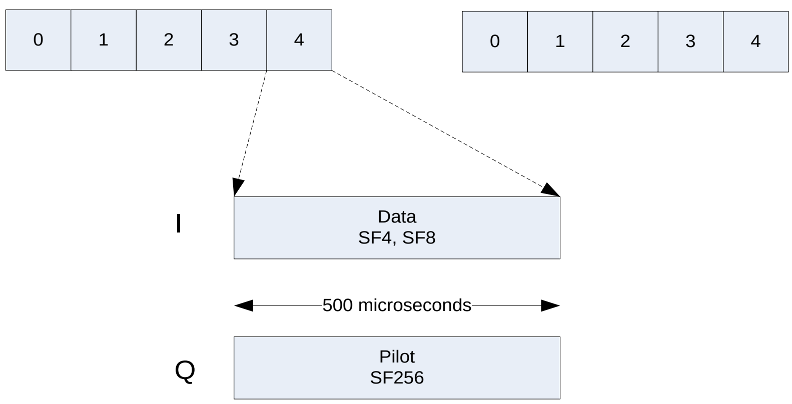

Figure 1.8 Proposed Slot Format - DL and UL

A maximum of 4 users can be served by the SBS when the SF=4, or 8 users when the SF=8. Each user, u, is assigned a pseudo noise (PN) sequence of N_c chips defined as:

$$c_u[n], n = [0; 1: \dots . N_c - 1] \tag{1.2}$$

$c_u[n]$ is the n_{th} chip where elements of c_u are +/- 1. Assuming the system is sampled at the chip rate, transmission is represented as:

$$x_u[n] = s_u[i]c_u[n\{modN_c\}] \tag{1.3}$$

where $s_u[i]$ is the ith information bearing signal, lasting for N_c chips. The signal in the presence of noise is received as:

$$r[n] = \sum_u \sqrt{P_u} \sum_l h_u[n - \tau_{u,l}]\, x_u[n - \tau_u - l] + \omega[n] \tag{1.4}$$

where $h_u[n, l]$=user u's channel response. τ_u is the integer delay of user u and $\omega[n]$ is additive noise.

1.3.2.1 Coherence Time

The coherence time ($T_{coh} = \frac{c}{f_c v} = \frac{1}{f_m}$) tells us tells us the time that the channel remains constant due to the effects of Doppler (f_m). Assuming carrier frequencies (f_c) of 28GHz and 72GHz with a maximum UE velocity (v) in the small cell of 0.5km/h, coherence times of 77ms and 30ms respectively are given. This tells us that the channel will remain constant over the duration of many 500μs slot periods which will help to minimise the amount of CSI required.

1.3.2.2 Channel Parameter Estimation –Proposed Algorithm

Both proposed architectures will require estimation of CSI (channel estimation) and significantly estimation of the multipath delay components (multipath search estimation). In both transmit and receive, data and pilot are separately BPSK modulated on the I and Q channel respectively, thus forming a QPSK constellation. Orthogonal variable spreading factor (OVSF) codes can be used on the pilot and data to maintain orthogonality. Different users use different UL scrambling codes to create a unique traffic channel. Neglecting mutual interference between the data and pilots, the signal received at the base station can be separated into I and Q channels. The Q channel can be used to estimate the channel parameters.

UL signals from the users are received by an N-element antenna array. With perfect instantaneous power control, to ensure all users exhibit equal power, an equivalent complex baseband expression of the composite received vector $\mathbf{X}(t)$ at time t is given by:

$$x(t) = \sum_{K=1}^{K} \sum_{l=1}^{L_k} \alpha_{k,l}^{u}\, e^{j\phi_{k,l}} \sum_{n=-\infty}^{\infty} b_k(n)c_k\big(t - nT_b - \tau_{k,l}\big)\, \overrightarrow{a_k}\big(\theta_{k,l}\big) + \mathbf{n}(t)$$
$$= \sum_{K=1}^{K} \sum_{l=1}^{L_k} \widehat{a_k}\big(\theta_{k,l}\big) \sum_{n=-\infty}^{\infty} b_k(n)c_k\big(t - nT_b - \tau_{k,l}\big) + \mathbf{n}(t) \quad (1.5)$$

where it is assumed that there are K users (one desired and K-1interfering users) the kth user has L_k propagation paths. The parameters $\alpha_{k,l}^{u}$, $\theta_{k,l}$, $\tau_{k,l}$ and $\theta_{k,l}$ are the UL amplitude, phase shift, time delay and angle of arrival of the lth multipath component respectively, from the kth user. $b_k(n)$ is the nth bit value, $c_k(t)$ is the spreading waveform assigned to the kth user, and T_b is the bit period. Assuming Architecture 1, the column vector $a_k\big(\theta_{k,l}\big) = \big[1, a_1\big(\theta_{k,l}\big), \ \ldots, a_{M-1}\big(\theta_{k,l}\big)\big]^T$ is the array response vector corresponding to the path arriving on angle $\theta_{k,l}$, where $a_m\big(\theta_{k,l}\big)$ is a complex number denoting the amplitude gain and phase shift of the signal at the (n+1)th antenna relative to that at the first antenna $\overrightarrow{a_k}\big(\theta_{k,l}\big) = \alpha_{k,l}^{u} e^{j\phi_{k,l}} \overrightarrow{a_k}\big(\theta_{k,l}\big)$ is the channel vector and $\mathbf{n}(t)$ is the additive white Gaussian noise vector.

$$P_{r=} \sum_{l=1}^{L_k} \big(\alpha_{k,l}^{u}\big)^2, for\ all\ K \quad (1.6)$$

P_r , is the total received power from the kth user and is assumed to be constant for all because of perfect instantaneous power control.

Following the beamformer, multipath search and estimation is performed. Assuming that the first user is the desired user and code synchronization has been established, the output of the, CMF results in the power delay profile of the desired user k_1) is given as [16]:

$$\mathbf{z}_1(\tau) = T_b b_1(n) \sum_{l=1}^{L_1} \widehat{a_k}\big(\theta_{1,l}\big)\delta\big(\tau - \tau_{1,l}\big) + \mathrm{s}_1(\tau) + \mathbf{m}_1(\tau) + \eta_1(\tau) \quad (1.7)$$

where $\mathrm{s}_1$is the self-interference signal vector due to other multipath components of the desired user, $\mathbf{m}_1$ is the MAI vector, and $\eta_1$is the thermal noise vector. The output of the matched filter is used to distinguish the desired signal from the co-channel interference who's time resolution is the chip interval or fraction of the chip interval T_c, depending on the oversampling factor.

The complexity of the CMF, assuming a parallel search of all timing uncertainties are searched for within the period of a chip, which is the optimal solution, is determined by the maximum delay spread searched over in nanoseconds. Assuming the delay spreads discussed in section Table 1.1 an average delay spread of 18ns can be expected for an indoor small cell.

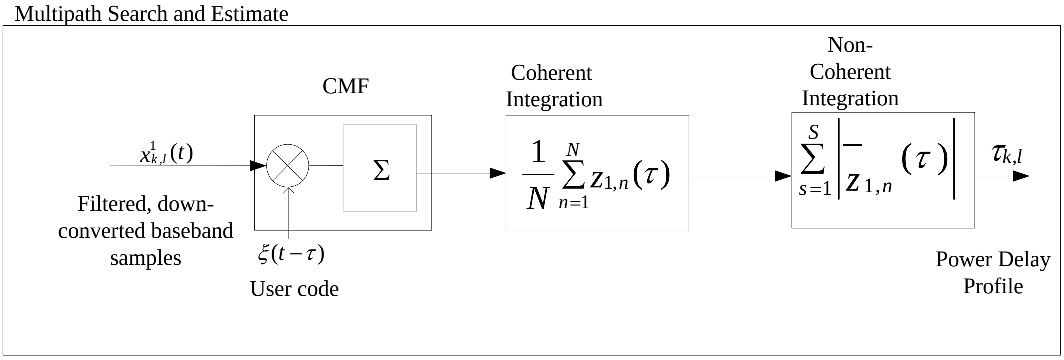

Figure 1.9 Multipath Estimation

Figure 1.8 shows that data is transferred in multiple slots where each slot comprises *N* pilot bits to aid channel and delay estimation and consider a slow fading channel. The delay profile for each pilot is first obtained, under the assumption that a long scrambling code is used. It is also noted that during a time slot period, the total phase change of the desired signal due to Doppler shift is small, if we assume a UE speed of 1km/h, and the slot period of T_{slot}=500μs (θ= f_d . 360˚. T_{slot}). This enables the use of coherent accumulation of the pilot chips, to obtain the mean delay profile of the user. With this approach, the mean delay profile, $\bar{z}_1$, is given by:

$$\bar{z}_1(\tau) = \frac{1}{N}\sum_{n=1}^{N} z_{1,n}(\tau) \tag{1.8}$$

where $z_{1,n}(\tau)$ is the CMF output of the *n*th pilot bit. Coherent integration will be applied to the time bins corresponding to the delay times of the desired user's multipath and will be accumulated *N* times [16]. In addition to coherent integration, and to further reduce the MAI a, non-coherent integration of the absolute value of the mean delay profile, $\bar{z}_1$, over the S timeslots is performed as follows:

$$\bar{\bar{z}}_1(\tau) = \frac{1}{S}\sum_{s=1}^{S} |\bar{z}_1(\tau)| \tag{1.9}$$

1.3.2.3 Multipath Search Estimation - Complexity

Determination of complexity can be broken down into two distinct timing acquisition functions:

- UE timing acquisition
- Multipath timing detection

Both these functions are determined by cross correlating the incoming received chips, or fractions of chips, with a local copy of the spreading and scrambling code sequence. The operations involve signbit complex correlations. The number of these operations, so called hypotheses [14], is determined by the round trip delay between the transmitter and receiver and the delay spread. These are therefore minimised in a small cell where the round trip delay is proportional to the cell size in the order of metres - $d_{rt} = T_c C/2$, where d_{rt} is the round trip delay distance in metres corresponding to T_c, the chip duration. Multipath delay spread can be assumed to be an average of 18ns based on Table 1.1. Considering a chip rate frequency of 2Gcps, the round trip delay incurred by each chip would be 0.15m. With a maximum coverage of 10m, a timing search with timing uncertainty of 133.33 chips would be required. Beyond this an additional 18ns of delay spread needs to be accounted for which results in a complex correlator of 169 taps ($T_{\mathrm{d}} = 84ns$).

The timing acquisition process involves testing all likely hypotheses. Traditionally, in large cell coverage areas, resource limitations meant that the hypotheses testing would be performed in a serial manner where each incorrect hypothesis is eliminated before the next one is tested [14]. Performing the operation in a parallel fashion increases the complexity meaning that for every chip, or fraction of a chip, received all possible timing uncertainties could be tested at once i.e. for the timing uncertainty above, 169 complex correlation operations would be made in 1 chip duration, T_c=0.5ns. The UE speed will also have an impact on how the timing acquisition is performed. Considering a UE in a small cell with a maximum velocity of 1km/h, a maximum movement per chip period, T_c, would be in the order of 13.5nm (13.5nm/chip) meaning an equivalent chip fraction of (T_cC/13.5e-9) ~=11.1e6 times smaller. In other words it would take 0.0055s for the timing uncertainty to move by 1 chip. A minimum search update frequency of 180Hz would therefore be required.

1.4 Energy Efficiency of the Proposed Architectures

At face value, the 2D rake system appears low in complexity in terms of baseband operations. For example the spreading and scrambling operations include single bit modulo-2 add operations, as shown in Figure 1.10.

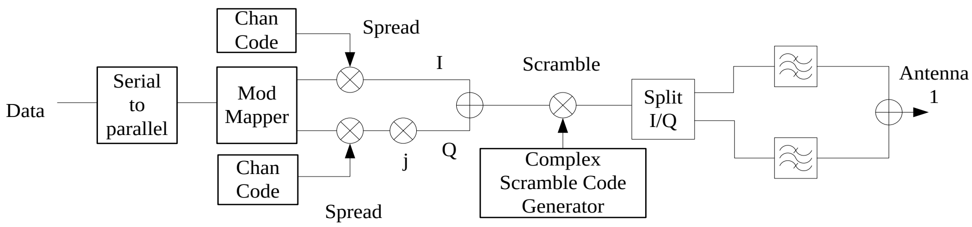

Figure 1.10 Spreading and Scrambling Operations

With the expected Gbits/s data rates anticipated for 5G systems, the circuit power P_c will play an increasingly important role in determining the energy efficiency of applicable architectures. As the bandwidth increases, so does the internal clocking of digital signal processor and associated digital and analogue hardware, leading to an increase in power usage. It is therefore prudent to rigorously consider circuit power consumed by signal processing.

The non-RF internal power, P_c, is expended on the antenna array critical computations and on all other operations such as analogue electronics and A/D and D/A conversions and is given as [21]:

$$P_c = \frac{2R_{flops}}{a} + Mb \tag{1.10}$$

where $R_{flops,}$ is the total computational rate in floating point operations per second (FLOPS) required by the critical computations, a is the power efficiency of computing measured in flops/watt given as 12.8 GFLOPS/W [21]. The factor of two for R_{flops} is intended to account for power required for read/write operations. M is the number of antennas and b is the internal non-RF power consumption associated with each antenna. Since there is uncertainty as to how much internal power is used a wide range of values of b can used. b (in mW) = 32, 64, 128, 256, 512, 1024, 2048, 4096.

For both architecture 1 & 2, it can be assumed that the critical computations will be the spreading and scrambling in the DL. Whereas in the UL, descrambling, despreading and complex correlation operations (for multipath timing acquisition) will dominate. As in OFDM, the 2D-Rake will be dominated by the number of complex multiplications. However, in practice many of these will include single bit multiplicands, for example modulo-2 additions for spreading. Assuming all operations are treated as full word size complex multiplies, an equivalent DL complexity for the 2D-Rake slot, per SBS j, can be given as:

$$R_{\mathrm{flops},j,DL} = M_j\left[K_J\,\frac{T_{\mathrm{slot}}}{T_{\mathrm{c}}}\right] \tag{1.11}$$

and for the UL:

$$R_{\mathrm{flops},j,UL} = \ M_j\left[K_J\left(\frac{T_{\mathrm{slot}}}{T_{\mathrm{c}}} + \frac{T_{\mathrm{p}}}{T_{\mathrm{c}}}\frac{T_{\mathrm{d}}}{T_{\mathrm{c}}}\right)\right] \tag{1.12}$$

where the UL operations are a combination of despreading together with timing uncertainty search functions associated with the multipath estimation process shown in Figure 1.9. Equation (1.12) assumes the use of a optimul implementation using a parrallel CMF.

Table 1.4 2D-Rake Operating Parameters

K_J: Users simultaneously served per SBS	4, 8
M_J: No. of antennas per SBS	2, 4
T_{slot}: Slot length	500μs
T_{c}: Chip Interval	0.5ns
T_{P}: Pilot Interval	500μs
T_{d}= Timing uncertainty, (dependent on the cell size and delay spread)	84ns

As was discussed in section 1.3.2.3, the rate at which the multipath detection is performed does not need to be continual. To provide the appropriate power consumed in 1 second, equation (1.12) can be extended to include a specified search rate R_s in Hz.

$$R_{\text{flops},j,UL} = M_j \left[K_J \left(\left(\frac{T_{\text{slot}}}{T_{\text{c}}} \right) 1/T_{\text{slot}} + \left(\frac{T_{\text{p}}}{T_{\text{c}}} \frac{T_{\text{d}}}{T_{\text{c}}} \right) R_s \right) \right] \tag{1.13}$$

Referring to the relationship between SE and EE expression (1.14)

$$\eta_{EE} = \frac{W_{\eta_{SE}}}{P_c + N_0 W (2^{\eta_{SE}} - 1)/\rho} \tag{1.14}$$

the impact of the circuit complexity can be determined. Figure 1.11 shows the SE-EE trade-off as a function of the search rate for both UL and DL processing of the SBS (Architecture 1). As previously indicated, and due to the relative slow movement of the indoor users, the multipath estimation process does not require continual updates. The graph shows dramatic increases in EE when the rate is reduced to 180Hz or 50Hz where a significant resultant lower power is achieved - (Architecture 1, BW=1GHz, *b*=32mW, a=12.8GFLOPS/W, PA efficiency=25%, number of users=4, number of baseband paths=1).

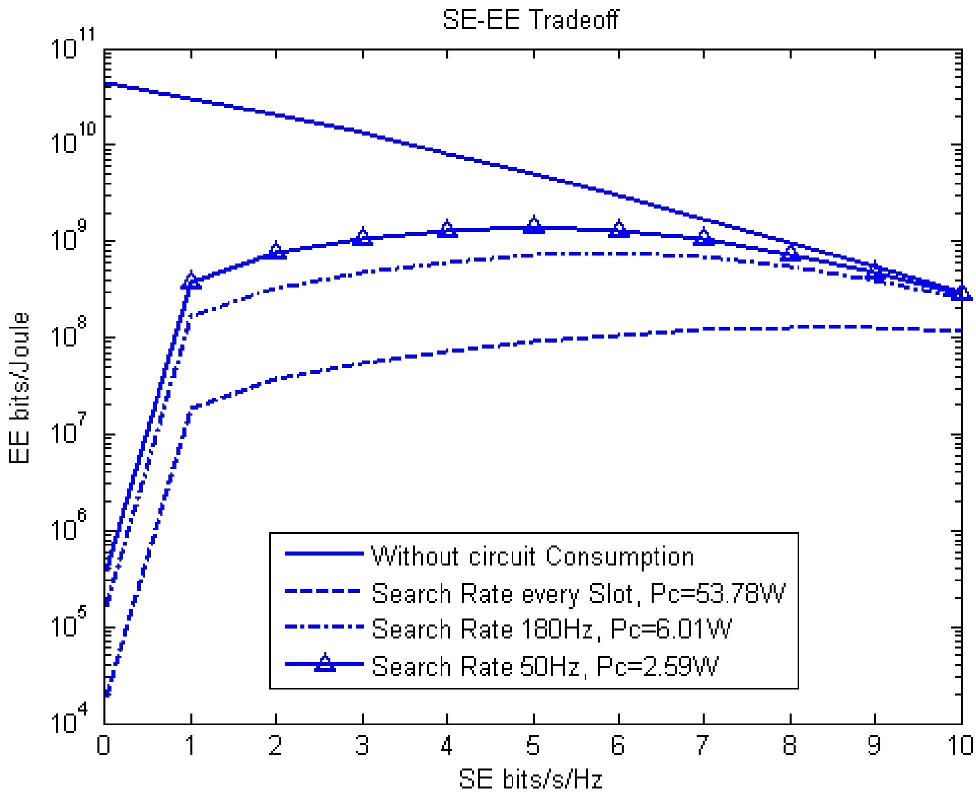

Figure 1.11 2D-Rake SE/EE trade-off as a function of Search Rate - Architecture 1

An equivalent graph for Architecture 2 is shown in Figure 1.12 and assumes the use of transmit diversity in the DL and receive diversity in the UL. In this case the baseband complexity is doubled as is the internal, non-RF generating circuitry power, *b*. (Architecture 2, BW=1GHz, *b*=32mW, a=12.8GFLOPS/W, PA efficiency=25%, number of users=4, number of baseband paths=2).

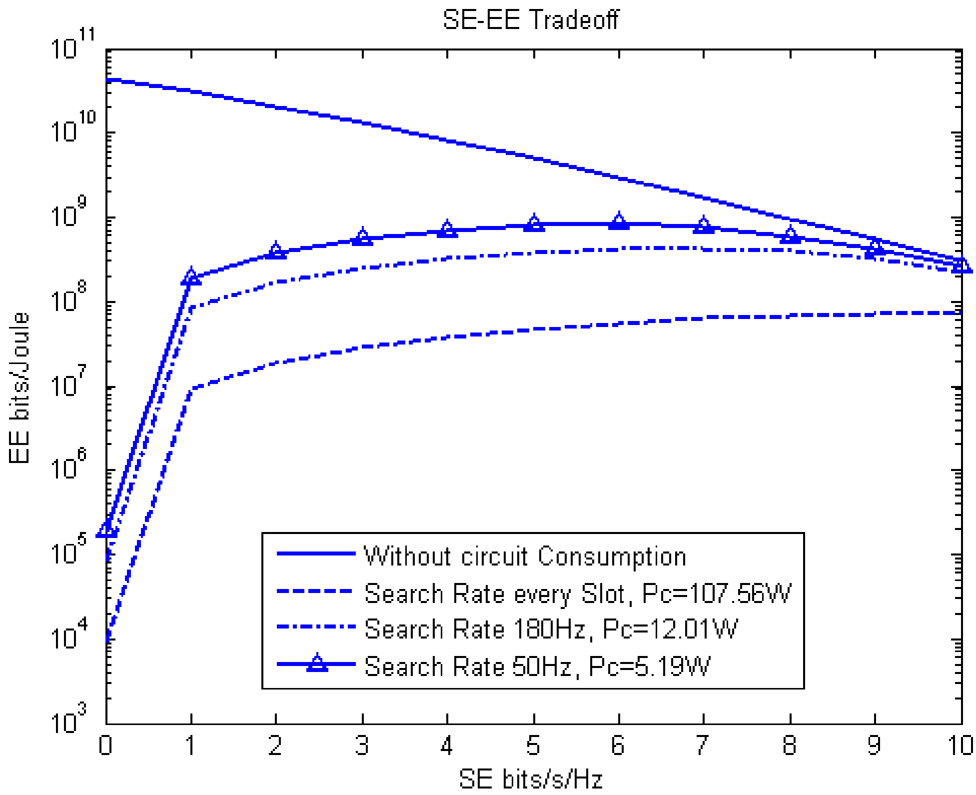

Figure 1.12 2D-Rake SE/EE trade-off as a function of Search Rate - Architecture 2

1.4.1 Comparison with 4G

To determine the suitability of the of the 2D-Rake architectures for their power and energy efficiency, it is useful to make comparisons with current fourth generation base stations, based on the LTE standard which comprises OFDM techniques on the DL and UL at the BS. With reference to the material presented in [20], appropriate transmit and received baseband operations and power can be determined for an LTE based femtocell base station (FBS). The authors assume a 40GOPS/W as the reference figure to determine the power (P) used. This is based on both the base station type and the underlying silicon feature size/geometry which was 65nm in 2010. The figure is scaled up 3 times for the FBS based on the assumption that more power efficient dedicated hardware would be used. An illustrative LTE block diagram is given in Figure 1.13 which shows the main baseband components. In addition, a halving of total dynamic power is attributed to a change from 65nm to 45nm complementary metal oxide semiconductor (CMOS) technology.

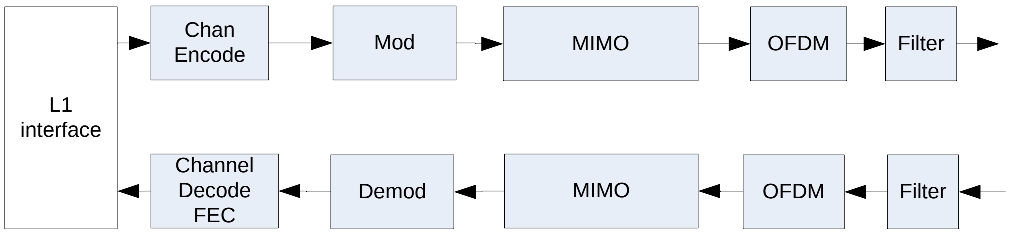

Figure 1.13 LTE SBS Main Baseband Processing Components

Total power consumed by the BS station comprises digital baseband (BB), RF (analogue), power amplifier and overhead (power systems and cooling)[20]:

$$P_{total} = P_{\mathrm{BB}} + P_{\mathrm{RF}} + P_{\mathrm{PA}} + P_{\mathrm{overhead}} \tag{1.15}$$

For the purposes of indoor SBSs the power associated with cooling can be ignored. In addition, the generation of power e.g. AC-DC and DC-DC conversion is omitted from this analysis to be comparative with the 2D-Rake analysis presented earlier.

Using appropriate power and scaling tables given in [20], based on the following expression (1.16) the power consumed for a desired set of key baseband sub-components can be determined, namely: filter: up/down sampling and filtering, OFDM: FFT and OFDM-specific processing, Frequency domain (FD) processing, mapping, MIMO equalization, forward error correction (FEC).

$$P_{\mathrm{total}} = \sum_{i \in I_{BB}} P_{i,\mathrm{ref}} \prod_{x \in X} \left(\frac{x_{act}}{x_{ref}}\right)^{s_{i,x}} + \sum_{i \in I_{RF}} P_{i,\mathrm{ref}} \prod_{x \in X} \left(\frac{x_{act}}{x_{ref}}\right)^{s_{i,x}} + P_{\mathrm{PA}} + P_{\mathrm{Overhead}} \tag{1.16}$$

Considering the complexity of an LTE SBS: Assuming the power of the frequency domain linear processing of a 20MHz, 4x4MIMO, 16-QAM, coding rate 1, with a 100% of time-domain duty cycle and a 100% frequency occupation, the power can be computed from (1.15) as:

$$P_{\mathrm{FD.lin}} = P_{\mathrm{FD.lin,ref}} \left(\frac{BW_{\mathrm{act}}}{BW_{\mathrm{ref}}}\right)^{s_1} \left(\frac{M_{\mathrm{act}}}{M_{\mathrm{ref}}}\right)^{s_2} \left(\frac{R_{\mathrm{act}}}{R_{\mathrm{ref}}}\right)^{s_3} \left(\frac{Ant_{\mathrm{act}}}{Ant_{\mathrm{ref}}}\right)^{s_4} \left(\frac{dt_{\mathrm{act}}}{dt_{\mathrm{ref}}}\right)^{s_5} \left(\frac{df_{\mathrm{act}}}{df_{\mathrm{ref}}}\right)^{s_6} \tag{1.17}$$

where n_{act} and n_{ref} referred to the actual system component under scrutiny and the reference system (20MHz, single antenna, 64-QAM, coding rate 1, 100% time domain and frequency domain duty cycling) respectively. **s** is the scaling vector (1 or 0). Where *BW* in the bandwidth, *M* is the modulation index, *R* is the FEC coding rate, *Ant* is the number of antennas, *dt* is the time-domain duty cycling and *df* is the frequency domain duty cycling.

Using the power required for DL linear processing ($P_{\text{FD.lin,ref}}$=0.166W, with 120GOPS/W in 65nm technology), and assuming that the FBS/SBS employs highly efficient integration of signal processing with power efficient dedicated hardware, we have the following power estimation (1.18). This assumes a 10MHz bandwidth, 64-QAM, 4 antennas, 100% time and frequency domain duty cycling and an FEC code rate of 1.

$$= 0.167\text{W x} \left(\frac{10}{20}\right)^{1} \left(\frac{6}{6}\right)^{0} \left(\frac{1}{1}\right)^{0} \left(\frac{4}{1}\right)^{1} \left(\frac{100}{100}\right)^{1} \left(\frac{100}{100}\right)^{1} = 0.334\text{W} \tag{1.18}$$

Completing the analysis of the LTE SBS baseband based on the approach above, using (1.17) gives approximated total power attributed to the baseband as per Table 1.5.

Table 1.5 Baseband Power – LTE SBS (10MHz, 64QAM, 4 antennas, ½ rate Turbo)

UL/DL **UL**	Ref (GOPS)	Power (W), 65nm, 2010	Power (W), 45nm,2010
Filter (inc D/C)	150	2.5	1.25
OFDM	60	1	0.5
FD Lin	30	0.5	0.25
FD non-lin	10	0.167	0.083
FEC	110	1.833	0.917
DL			
Filter	100	1.667	0.833
OFDM	60	1	0.5
FD lin	20	0.333	0.167
FD non-lin	5	0.333	0.167
FEC	20	0.333	0.167
Total Power (W)		9.667	4.833

Factoring in the transceiver into (1.10) and considering a range of values for *b* to be between 32 - 4096mw, increases the overall power as Table 1.6. The Energy Consumption Ratio ECR (1.19) is given based on a theoretical bitrate of 480Mbits/s where E is the energy required to deliver M bits of information over time T, and $D = M/T$ is the data rate in bits per second.

$$ECR = \frac{E}{M} = \frac{PT}{M} = \frac{P}{D}\ [J/bit] \tag{1.19}$$

Table 1.6 Total Power – LTE (10MHz, 64QAM, 4 antennas, ½ rate) Turbo)

Transceiver power, b, (mw)	Total Power (W), 65nm, 2010	ECR J/bit	Total Power (W), 45nm, 2012	ECR J/bit
32	9.795	2.04E-8	4.961	1.03E-8
64	9.923	2.07E-8	5.089	1.06E-8
128	10.179	2.12E-8	5.345	1.11E-8
256	10.691	2.23E-8	5.857	1.22E-8
512	11.715	2.44E-8	6.881	1.43E-8
1024	13.763	2.87E-8	8.929	1.86E-8
2048	17.859	3.72E-8	13.025	2.71E-8
4096	26.051	5.42E-8	21.217	4.42E-8

1.4.1.1 2D-Rake

The 2D-rake power calculated above, considered a power efficiency of the 12.8GFLOPS/W. In order to make a comparison with the LTE system, the power efficiency of 120 and 240GOPS/W should be used. Based on this, the results are shown in Table 1.7 and Table 1.8 for both Architecture 1 and Architecture 2. ECR is provided based on the link budget shown in Table 1.2 and assumes a 10m cell at 28GHz. The use of state of the art mmWave ADC/DAC components, [22][23] (which include the necessary up and down conversion) are included in the total power. A search rate of 180Hz is assumed.

Table 1.7 Baseband and Transceiver Power – Architecture 1

Transceiver power, *b*, (mw)	Arch 1 power (W), 65nm, 2010	ECR J/bit	Arch 1 power (W), 45nm, 2012	ECR J/bit
32	4.70	1.51E-9	4.38	1.41E-9
64	4.77	1.54E-9	4.45	1.43E-9
128	4.89	1.57E-9	4.57	1.47E-9
256	5.15	1.66E-9	4.83	1.56E-9
512	5.66	1.82E-9	5.34	1.72E-9
1024	6.69	2.16E-9	6.37	2.05E-9
2048	8.73	6.71E-9	8.41	2.71E-9
4096	12.83	4.13E-9	12.51	4.03E-9

Table 1.8 Baseband and Transceiver Power – Architecture 2

Transceiver power, *b*, (mw)	Arch 2 power (W), 65nm, 2010	ECR J/bit	Arch 2 power (W), 45nm, 2012	ECR J/bit
32	9.34	3.01E-9	8.7	2.80E-9
64	9.4	3.03E-9	8.77	2.33E-9
128	9.53	3.07E-9	8.89	2.87E-9
256	9.79	3.15E-9	9.15	2.95E-9
512	10.3	3.32E-9	9.66	3.12E-9
1024	11.32	3.65E-9	10.69	3.45E-9
2048	13.37	4.31E-9	12.73	4.11E-9
4096	17.47	5.63E-9	16.83	5.43E-9

1.4.1.2 SE-EE Tradeoff 4G vs. 5G

Based on the overall circuit power consumption calculated above for the LTE FBS, 2D-Rake architecture 1 and 2D-Rake architecture 2, the SE-EE tradeoff is shown in Figure 1.14. Circuit powers assume worst case transceiver power for all architectures.

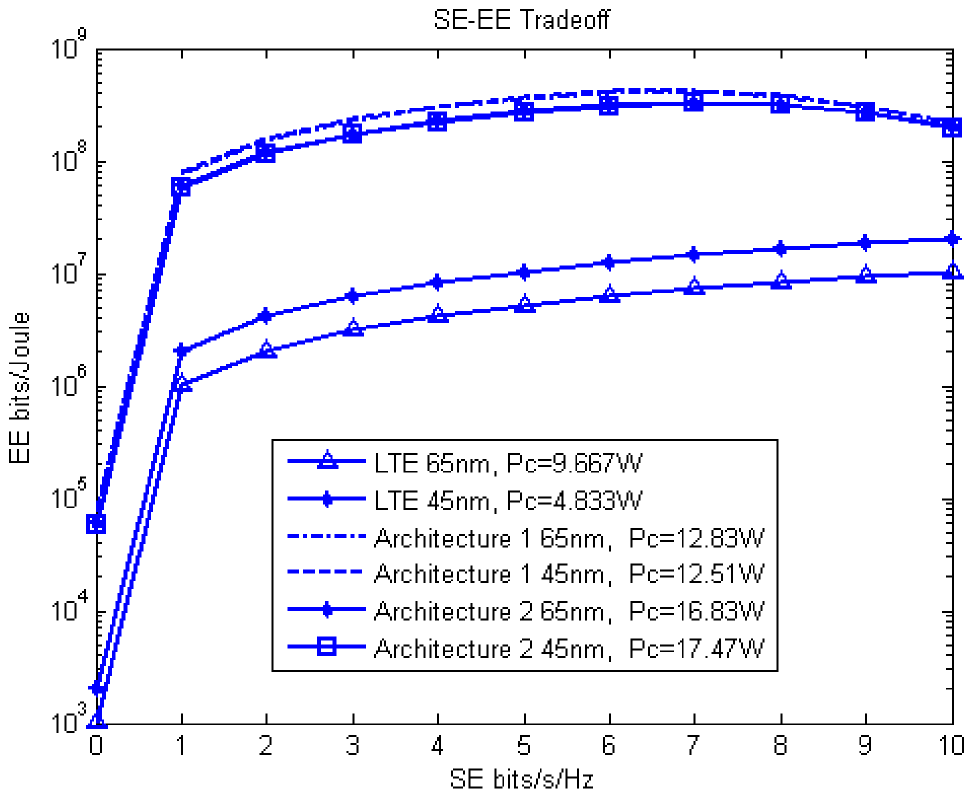

Figure 1.14 4G LTE vs. Proposed 5G Architectures

Based on these results, both 2-D Rake architectures are shown to provide superior performance and improve the energy consumption. Significantly, EE-SE tradeoff is shown to improve by an order of magnitude. The complexity analysis of the 2D-Rake architectures concentrated heavily on the baseband, however realistic ADC and DAC powers were included in the analysis. The use of RF beamforming means that the only a single ADC and DAC are used in the implementation.

1.5 Conclusions

This chapter has analysed the possible air interface approaches suitable for indoor small cell use. With energy efficiency being critical, the use of multiple antenna beamforming may be limited to a small number of antennas resulting in a wider beamwidth and therefore subject to multipath and ISI. To exploit this, the use of direct sequence spread spectrum using a Rake combiner is analysed. The Rake combiner used in conjunction with a moderate number of beamforming antennas is shown to give good theoretical performance as well as providing gain from the multipath. The Rake combiner therefore acts as the equaliser. Two architectures are presented: one using a single chain RF beamformer and one using transmit and receive diversity. The complexity of the solutions was analysed in detail to provide an anticipated power usage based on the physical layer signal processing operation. The impact of multipath search resolution was shown to adversely impact power consumption, but based on an analysis of the search rate required in the small cell, dramatic reductions in total power were shown. Finally, the solutions were compared to that of present day 4G LTE technology for their power usage and energy efficiency. Results showed improved Energy Consumption Ratio for the two candidate architectures and provided a SE-EE tradeoff significantly better than a current generation 4G FBS by an order of magnitude.

References

[1] Da Silva, I.; Mildh, G.; Rune, J.; Wallentin, P.; Vikberg, J.; Schliwa-Bertling, P.; Rui Fan, "Tight Integration of New 5G Air Interface and LTE to Fulfill 5G Requirements," *Vehicular Technology Conference (VTC Spring), 2015 IEEE 81st* , vol., no., pp.1,5, 11-14 May 2015.

[2] Dahlman, E.; Mildh, G.; Parkvall, S.; Peisa, J.; Sachs, J.; Selén, Y.; Sköld, J., "5G wireless access: requirements and realization," in *Communications Magazine, IEEE* , vol.52, no.12, pp.42-47, December 2014.

[3] Demestichas, P.; Georgakopoulos, A.; Karvounas, D.; Tsagkaris, K.; Stavroulaki, V.; Jianmin Lu; Chunshan Xiong; Jing Yao, "5G on the Horizon: Key Challenges for the Radio-Access Network," *Vehicular Technology Magazine, IEEE* , vol.8, no.3, pp.47,53, Sept. 2013.

[4] Larew, S.G.; Thomas, T.A.; Cudak, M.; Ghosh, A., "Air interface design and ray tracing study for 5G millimeter wave communications," in *Globecom Workshops (GC Wkshps), 2013 IEEE* , vol., no., pp.117-122, 9-13 Dec. 2013.

[5] T. Marzetta, "Noncooperative cellular wireless with unlimited numbers of base station antennas," Wireless Communications, IEEE Transactions on, vol. 9, no. 11, pp. 3590–3600, November 2010.

[6] Rowell, C.; Shuangfeng Han; Zhikun Xu; I Chih Lin, "Green RF technologies for 5G networks," in *Wireless Symposium (IWS), 2014 IEEE International* , vol., no., pp.1-4, 24-26 March 2014.

[7] Zhouyue Pi; Khan, F., "An introduction to millimeter-wave mobile broadband systems," *Communications Magazine, IEEE* , vol.49, no.6, pp.101,107, June 2011.

[8] K.AO-Cheng Huang, Zhaooheng Wang, "Beam Steering Antenna" in Millimeter Wave Communication Systems. IEEE / J.Wiley & Sons, 2012.

[9] Rappaport, T.S.; Shu Sun; Mayzus, R.; Hang Zhao; Azar, Y.; Wang, K.; Wong, G.N.; Schulz, J.K.; Samimi, M.; Gutierrez, F., "Millimeter Wave Mobile Communications for 5G Cellular: It Will Work!," *Access, IEEE* , vol.1, no., pp.335,349, 2013.

[10] S. Deng, C. J. Slezak, G. R. MacCartney, Jr., and T. S. Rappaport, ``Small Wavelengths Big potential: Millimeter wave propagation measurements for 5G," *Microw. J.*, Nov. 2014.

[11] Anderson, C.R.; Rappaport, T.S., "In-building wideband partition loss measurements at 2.5 and 60 GHz," in *Wireless Communications, IEEE Transactions on* , vol.3, no.3, pp.922-928, May 2004.

[12] Manabe, T.; Miura, Y.; Ihara, T., "Effects of antenna directivity and polarization on indoor multipath propagation characteristics at 60 GHz," in *Selected Areas in Communications, IEEE Journal on* , vol.14, no.3, pp.441-448, Apr 1996.

[13] Sawaya, W.; Clavier, L., "Simulation of DS-CDMA on the LOS multipath 60 GHz channel and performance with RAKE receiver," in *Personal, Indoor and Mobile Radio Communications, 2003. PIMRC 2003. 14th IEEE Proceedings on* , vol.2, no., pp.1232-1236 vol.2, 7-10 Sept. 2003.

[14] Rendevski, N.; Cassioli, D., "60 GHz UWB rake receivers in a realistic scenario for wireless home entertainment," in *Communications (ICC), 2015 IEEE International Conference on* , vol., no., pp.2744-2749, 8-12 June 2015.

[15] Andrew. J. Viterbi, "Modulation and demodulation of spread spectrum signals", CDMA Principles of Spread Spectrum Communications 3rd ed. Chichester, U.K.: Addison Wesley, 1996, pp. 77_121.

[16] Hsueh-Jyh Li; Ta-Yung Liu, "Comparison of beamforming techniques for W-CDMA communication systems," in *Vehicular Technology, IEEE Transactions on* , vol.52, no.4, pp.752-760, July 2003.

[17] Singh, J.; Ponnuru, S.; Madhow, U., "Multi-Gigabit communication: the ADC bottleneck[1]," *Ultra-Wideband, 2009. ICUWB 2009. IEEE International Conference on* , vol., no., pp.22,27, 9-11 Sept. 2009.

[18] Muirhead, D.; Imran, M.A.; Arshad, K., "Insights and Approaches for Low-Complexity 5G Small-Cell Base-Station Design for Indoor Dense Networks," in *Access, IEEE*, vol.3, no., pp.1562-1572, 2015.

[19] Ghosh, A.; Thomas, T.A.; Cudak, M.C.; Ratasuk, R.; Moorut, P.; Vook, F.W.; Rappaport, T.S.; MacCartney, G.R.; Shu Sun; Shuai Nie, "Millimeter-Wave Enhanced Local Area Systems: A High-Data-Rate Approach for Future Wireless Networks," *Selected Areas in Communications, IEEE Journal on* , vol.32, no.6, pp.1152,1163, June 2014.

[20] Desset, C.; Debaillie, B.; Giannini, V.; Fehske, A.; Auer, G.; Holtkamp, H.; Wajda, W.; Sabella, D.; Richter, F.; Gonzalez, M.J.; Klessig, H.; Godor, I.; Olsson, M.; Imran, M.A.; Ambrosy, A.; Blume, O., "Flexible power modeling of LTE base stations," in *Wireless Communications and Networking Conference (WCNC), 2012 IEEE* , vol., no., pp.2858-2862, 1-4 April 2012.

[21] Hong Yang; Marzetta, T.L., "Total energy efficiency of cellular large scale antenna system multiple access mobile networks," in *Online Conference on Green Communications (GreenCom), 2013 IEEE* , vol., no., pp.27-32, 29-31 Oct. 2013.

[22] ADC12J4000 12-Bit 4 GSPS ADC With Integrated DDC12-Bit. http://www.ti.com/lit/ds/symlink/adc12j4000.pdf

[23] DAC39J84 Quad-Channel, 16-Bit, 2.8 GSPS, Digital-to-Analog Converter. http://www.ti.com/lit/ds/symlink/dac39j84.pdf